

Simulations of Jet Fuel Thermal Oxidative Degradation: Part I. The Effect of Metal Surface Catalysis on the Thermal Oxidation of Jet Fuel

Thammarat Duangthip^{1*}, Jamie S. Ervin²

¹Department of Mechanical Engineering, Asian University of Science and Technology,
89 Moo 12, Highway 331, Huay Yai, Banglamung, Chonburi 20260, Thailand
Tel: 0-3875-4450, Fax: 0-3875-4460, *E-mail: thammaratd@asianust.ac.th

²University of Dayton Research Institute, 300 College Park, Dayton, OH 45469-0210, USA
Tel: 1-937-252-8878 Ext 114, Fax: 1-937-252-9917, E-mail: jamie.ervin@notes.udayton.edu

Abstract

Jet fuel is used for cooling in high performance aircraft. Unfortunately, jet fuel reacts with dissolved O₂ in the presence of heat to form unwanted surface deposits. Computational fluid dynamics incorporating pseudo-detailed chemical kinetics with a wall reaction is used to simulate the effects of treated and untreated stainless-steel surfaces on liquid phase thermal-oxidation of jet fuel in both isothermal and non-isothermal heated tube experiments. A hydroperoxide decomposition reaction is used to represent the surface chemistry. The effects of a treated surface on thermal-oxidation were modeled by adjusting the activation energy of the surface reaction. Non-isothermal heated tube experiments which measure dissolved O₂ are performed here while isothermal flow experiments are performed elsewhere. Simulations of dissolved O₂ consumption in the presence of treated and untreated surfaces which include the wall reaction agree reasonably well with the dissolved O₂ measurements.

Key Words: Jet fuel, Thermal oxidative degradation, Numerical simulation.

1. Introduction

Jet fuel is used in military aircraft for purposes of cooling before it is burned in the combustor. As fuel flows through the fuel system, an autoxidation chain involving heteroatomic fuel species proceeds, which results in the reaction of dissolved O₂ and the formation of oxidized products [1]. Oxidized products may subsequently react to form surface deposits which reduce fuel flow and degrade heat transfer effectiveness. Moreover, catastrophic engine failure could occur if these deposits impair the operation of close-tolerance valves. Thus, it is important to study liquid phase fuel oxidation and the involved surface reactions. Computational fluid dynamics together with chemical kinetics can show aircraft engine designers how the fluid dynamics and heat transfer influence fuel oxidation and accompanying surface reactions. Three different types of chemical kinetic mechanisms have been used to simulate jet fuel thermal-oxidation: global mechanisms, detailed

mechanisms, and pseudo-detailed mechanisms [1, 2]. In general, global kinetic mechanisms have employed one reaction to represent jet fuel thermal-oxidation:



Although jet fuel thermal-oxidation actually involves several reactions, the basic assumption of Eq. (1) is that the overall reaction of a mixture of compounds can be represented by one rate equation. This rate equation consists of a rate constant multiplied by concentrations having the form as in Eq. (2)

$$-\frac{d[\text{O}_2]}{dt} = k [\text{RH}][\text{O}_2]^n \quad (2)$$

In Eq. (2), the fuel is represented by a single compound RH. The rate constant k is represented by the product of an Arrhenius A factor and an activation energy term. In addition, the order of the reaction is given by n . Because individual fuel samples are different, the A factor and activation energy may have to be determined for different fuel samples.

While a global mechanism consists of relatively few reactions, a detailed kinetic mechanism may consist of hundreds of reactions to represent jet fuel thermal-oxidation. Moreover, a detailed kinetic mechanism would include a multitude of species that exist within the fuel. These species and their concentrations will change for each fuel sample. Thus, a detailed mechanism is not practical for the study of jet fuel thermal-oxidation that also employs computational fluid dynamics. An alternative approach that has been used to simulate thermal-oxidation of jet fuel is the use of a pseudo-detailed chemical kinetic mechanism. Pseudo-detailed chemistry represents the dominant chemistry and the behavior of classes of species within the fuel [1, 2, 3, 4]. Pseudo-detailed chemistry is midway in complexity between global and detailed kinetic mechanisms and was previously used with reasonable success in simulating the thermal-oxidation of jet fuels.

Due to their complexity, surface reactions have received little attention in previous computational studies of liquid phase jet fuel thermal-oxidation [1, 2, 3, 4]. Here we attempt to include the effects of surface catalysis on autoxidation. Isothermal experimental studies of the surface effects on jet fuel thermal-oxidation have shown that tubing with a surface treatment can delay dissolved O₂ consumption relative to that of stainless-steel [5]. This surface treatment involved the chemical vapor deposition of a proprietary silica-based layer (Silcosteel tubing) [6].

The slower oxidation rate suggests that a surface passivated by surface treatment with an inert coating could delay or significantly reduce surface deposition. It is desirable to simulate jet fuel thermal-oxidation using pseudo-detailed chemical kinetics and surface reactivity by including a wall reaction in the computational model. A goal of this work is to investigate if the surface catalyzed decomposition of fuel hydroperoxides can be used to simulate the influence of surface type on jet fuel thermal-oxidation. Studying the effects of a metal surface or a relatively inert surface on jet fuel oxidation is important because such research will ultimately assist the understanding of jet fuel surface deposition.

2. Simulation Methodology

2.1 Pseudo-Detailed Chemistry Kinetics. A pseudo-detailed chemical kinetic mechanism used to simulate the liquid phase oxidation of jet fuel was first proposed by Zabarnick [3]. Table 1 shows the present chemical kinetic mechanism, which consists of 17 bulk reactions and one wall reaction. The rate constant, k , for each reaction is represented in Arrhenius form

$$k = A e^{(-E_a/RT)} \quad (3)$$

In Eq. (3), A is the pre-exponential factor, E_a is the activation energy, R is the universal gas constant, and T is the temperature.

Reactions 1-4 and reaction 10 of Table 1 comprise a simple chain mechanism involving the formation of free radicals due to hydrocarbon fuel oxidation. In reaction 1, species I is used to initiate the complex process that

forms the free radical R[•] at a low reaction rate. Reaction 1 becomes negligible relative to other reactions once the chain begins. The single compound RH represents the bulk fuel and is assumed to have the chemical properties of a straight-chain alkane, such as n-dodecane. Reactions 5-9 represent the antioxidant chemistry associated with the interception of an alkylperoxy radical by species AH. Species AH represents an antioxidant like butylated hydroxytoluene (BHT) that intercepts peroxy free radicals.

Reactions 11-16 represent alkylhydroperoxide decomposition chemistry, which occurs at a sufficiently high temperature and plays an important role in accelerated O₂ consumption in the bulk fuel. Reaction 17 represents the reaction of fuel hydroperoxides with the hydroperoxide decomposing

species, SH. SH is believed to include sulfur species (sulfides and disulfides, for example) that decompose fuel hydroperoxides into non-radical products. Previous simulations including only bulk reactions have shown that reaction 17 can slow the oxidation rate when fuel hydroperoxides in the bulk fuel react with SH species [4]. In addition, previous simulations have demonstrated that AH and SH can act synergistically to slow the oxidation rate [1, 4]. For simplicity, the pseudo-detailed chemical kinetic mechanism employs the concentration of antioxidants AH and SH to differentiate fuel samples.

Table 1. Present Pseudo-Detailed Chemical Kinetic Mechanism

No.	Reaction	Activation Energy: Kcal/mol	A Factor: mol, L, s
Bulk Reactions			
1	I → R [•]	1 x 10 ⁻⁷	0
2	R [•] + O ₂ → RO ₂ [•]	3 x 10 ⁹	0
3	RO ₂ [•] + RH → ROOH + R [•]	3 x 10 ⁹	10
4	RO ₂ [•] + RO ₂ [•] → termination	3 x 10 ⁹	0
5	RO ₂ [•] + AH → ROOH + A [•]	3 x 10 ⁹	5
6	AO ₂ [•] + RH → AO ₂ H + R [•]	3 x 10 ⁵	10
7	A [•] + O ₂ → AO ₂ [•]	3 x 10 ⁹	0
8	AO ₂ [•] + AH → AO ₂ H + A [•]	3 x 10 ⁹	6
9	AO ₂ [•] + AO ₂ [•] → products	3 x 10 ⁹	0
10	R [•] + R [•] → R ₂	3 x 10 ⁹	0
11	ROOH → RO [•] + •OH	1 x 10 ¹⁵	42
12	RO [•] + RH → ROH + R [•]	3 x 10 ⁹	10
13	RO [•] → R [•] _{prime} + carbonyl	1 x 10 ¹⁶	15
14	•OH + RH → H ₂ O + R [•]	3 x 10 ⁹	10
15	RO [•] + RO [•] → termination	3 x 10 ⁹	0
16	R [•] _{prime} + RH → alkane + R [•]	3 x 10 ⁹	10
17	ROOH + SH → products	3 x 10 ⁹	16
Wall reaction			
18	ROOH → RO [•] + •OH	1 x 10 ⁹	37-42

2.2 Wall Reaction. Using a modified version of the pseudo-detailed chemical kinetic mechanism, Ervin and Zabarnick simulated the thermal oxidation of jet fuel flowing within stainless-steel tubes with reasonable success [4]. In preliminary efforts during the current study, hydrocarbon oxidation on a passivated surface was simulated by using the activation energy for the unimolecular hydroperoxide decomposition reaction assumed to occur in the bulk fuel. Unfortunately, agreement between experiment and simulation could not be obtained. In numerical simulations of the effects of different surfaces on the thermal-oxidation of jet fuel, it is believed that the use of surface reactions rather than the arbitrary modification of bulk reactions is more representative of the actual chemistry. Simulations of reactions between a gas phase species and a metal

surface have commonly been performed by employing Langmuir-Hinshelwood mechanisms which have been reported to provide reasonable descriptions of the surface chemistry [7, 8, 9, 10, 11]. These mechanisms consist of three types of reactions: adsorption of molecules, reaction between adsorbed molecules (catalytic reaction), and desorption of adsorbed molecules. A variable number of site species on the active surface is required with their use. Thus, the physical and chemical properties of the site species on the active surface including their interactions with species in the fluid are usually known [7, 8, 9, 10, 11]. However, this is not the case for reactions between fuel hydroperoxides, which are known to have an important role in thermal oxidation, and the surface species of stainless-steel tubing. With stainless-steel tubes used in the present heated tube experiments, the active site species and their population are unknown. Although it is agreed that active metal ions (such as Fe, V, Mn, Ni, and Cu) comprising the surface play an important role in the catalysis of fuel hydroperoxide decomposition, little is known about the actual reactions between fuel hydroperoxides and site species on metal surfaces [12]. Moreover, adsorption and desorption processes on a real surface are extremely difficult, if not impossible, to model in detail in a computational fluid dynamics simulation [10, 11]. The present work does not consider the actual elementary surface reactions, which are unknown for the stainless-steel and treated (inert) surfaces used in this study. Instead, for simplicity, the complex surface reactions are represented by the single reaction



It is assumed that this hydroperoxide decomposition reaction is catalyzed by an active surface and has a lower activation energy than the corresponding reaction in the bulk fuel. As a result, the rate of reaction of fuel hydroperoxide decomposition on the surface may be higher than corresponding reactions in the bulk [5, 13, 14]. In addition, the reactions between fuel hydroperoxides and species comprising metal surfaces produce the free radical species, RO^\bullet and $\bullet\text{OH}$, which diffuse into the bulk liquid and further react increasing the local free radical pool [5, 13, 14].

In the present study, a wall reaction (reaction 18, Table 1) representing unimolecular alkylhydroperoxide decomposition is appended to the pseudo-detailed chemical kinetic mechanism of Ervin and Zabarnick [4]. The rate equation of the hydroperoxide decomposition reaction at the wall is given here as

$$-\frac{d[\text{ROOH}]}{dt} = A e^{-E_a/RT} [\text{ROOH}]^\alpha \quad (5)$$

In Eq. (5), α is the order of reaction for the hydroperoxide decomposition. In detailed studies of simple catalytic surface reactions, the order of the reaction is determined from the overall mechanism of the adsorption-surface reaction-desorption process [10,

11]. In this study, we do not have knowledge of these surface processes, so the value of α was adjusted to study its influence on fuel oxidation. The choice of the activation energy in Eq. (5) is used to represent the effects of a stainless-steel or passive surface on thermal oxidation of jet fuel flowing within a heated tube. In general, the activation energy of a surface reaction is lower than that of the corresponding bulk reaction [7, 8]. However for simplicity, the activation energy in Eq. (5) for the passive surface is selected to be 42 kcal/mol and is equal to that of the corresponding bulk hydroperoxide decomposition reaction [1]. Thus, flowing experiments which use the treated stainless-steel surface and a surrogate fuel can be performed to determine α and A for use in Eq. (5). In our approach, we assume that these values of α and A are equally valid for a stainless-steel surface. Although the E_a of the fuel hydroperoxide decomposition reaction for a stainless-steel surface is unknown, it must be less than the E_a of the more passive Silcosteel surface. Experiments were performed to determine reasonable values of E_a for a stainless-steel surface, and the selection of E_a for stainless-steel surfaces is described later in this paper.

2.3 Calibration of the Mechanism. In previous work, a "calibration" of the kinetic mechanism was performed by adjusting (within acceptable kinetic limits) the pre-exponential factors and activation energy of reactions 3 and 11 (Table 1) until the chemistry model reasonably represented the thermal oxidation of a hydrotreated fuel on a stainless-steel surface [4]. However, the hydrotreated fuel may likely have contained small concentrations of naturally occurring antioxidants that were not taken into account. It is important to make the mechanism independent of the initial antioxidant concentration and to reduce the influence of the surface material by using an inert surface. In the present work, a "calibration" is performed using computational fluid dynamics together with the pseudo-detailed chemical kinetic mechanism by simulating previous measurements of dissolved O_2 consumption using treated tubes (Silcosteel, 2.16-mm ID x 3.18-mm OD, heated length 0.813 m) under isothermal flow conditions (wall temperature 185 °C) [15, 16]. In these experiments, the average residence time of the fuel (Exxsol D110) in the heated tube was varied by adjusting the flow rate. Exxsol D110 (Exxon-Mobil) is a hydrocarbon solvent that is a combination of ~50%(wt) paraffins, ~50%(wt) cycloparaffin and <1%(wt) aromatics [15]. It contains little, if any, antioxidants and, thus, oxidizes very rapidly [15]. Moreover, Exxsol D110 has properties (density and viscosity, for example) similar to Jet A-1 and Jet A fuels [15, 16]. For reaction 1 (Table 1), the pre-exponential factor of $1 \times 10^{-7} \text{ s}^{-1}$ is selected for the representation of free-radical initiations occurring within Exxsol D110 in the current simulations. The use of this pre-exponential factor is reasonable as it is small enough to initiate the autoxidation chain but produces a negligible production of R^\bullet once the chain begins. Except for reactions 3 and 11 (Table 1), the pre-exponential factors and activation energies of the bulk reactions are the same as those used

in our previous computational fluid dynamics simulations [4]. With regard to reaction 11, the pre-exponential factor and activation energy originally used by Zabarnick to represent homogeneous ROOH decomposition are retained [3]. Thus for calibration of the mechanism, one rate parameter is adjusted within well-defined bounds. The activation energy of reaction 3 (Table 1) can range between 8-14 kcal/mol and is selected as 10 kcal/mol rather than 12 kcal/mol as used previously [1, 4]. In preliminary simulations, 10 kcal/mol was found to better represent the oxidation measurements.

The order of the surface reaction influences the oxidation rate of Exxsol D110. Therefore, it is important to consider the effects of varying the order of the surface reaction on the thermal-oxidation of Exxsol D110. When the order of the surface reaction is unity, the predicted oxidation rate of Exxsol D110 is slower than the measured oxidation rate. When α is decreased to 0.8, the dissolved O₂ is consumed more rapidly, and the predicted oxidation rates agree well with the measured rates. Decreasing α below unity increases the free-radical species concentration on the wall at a greater rate than when α is unity because the ROOH concentration is a fractional value here. When α is decreased below 0.8, the simulated oxidation rate is too rapid, and the simulated dissolved O₂ is completely consumed before the measured value. A pre-exponential factor of $1 \times 10^9 \text{ s}^{-1}$ was found to provide the best agreement between simulation and measurement of the dissolved O₂ consumption in Exxsol D110. This value for A lies within the range ($10^3 \text{ s}^{-1} - 10^{12} \text{ s}^{-1}$) of reported values for pre-exponential factors of metal surfaces [7, 12].

The above values of A and α are used in all simulations which follow. In addition, it is assumed for simplicity that the activation energy of the surface reaction is the same for all stainless-steels considered (SS316 and SS304).

2.4 Computational Fluid Dynamics Code. To understand the effects of temperature, flow, and surface material on thermal-oxidation, a commercially available computational fluid dynamics code (CFDACE) was used to simulate the flow and oxidative chemistry within a heated tube [17]. The fuel motion inside the tube was assumed to be axisymmetric and steady. To simulate the fuel chemistry within the heated tubes, the species, temperature, and velocity distributions were obtained by finite volume solution of the species, enthalpy, Navier-Stokes, and turbulent energy equations. The properties of the fuel (density, viscosity, thermal conductivity, specific heat, and enthalpy) depend on the fuel temperature. The governing equations written for a cylindrical (z, r) coordinate system are

$$\frac{\partial(\rho u)}{\partial z} + \frac{\partial(\rho v)}{\partial r} + \frac{\rho v}{r} = 0 \quad (6)$$

$$\frac{\partial(\rho u \Phi)}{\partial z} + \frac{\partial(\rho v \Phi)}{\partial r} = \frac{\partial}{\partial z} \left(\Gamma^\Phi \frac{\partial \Phi}{\partial z} \right) + \frac{\partial}{\partial r} \left(\Gamma^\Phi \frac{\partial \Phi}{\partial r} \right) - \frac{\rho v \Phi}{r} + \frac{\Gamma^\Phi}{r} \frac{\partial \Phi}{\partial r} + S^\Phi \quad (7)$$

Eq. (6) is the continuity equation, and Eq. (7) represents the momentum, species, turbulent energy ($k-\epsilon$), or

energy equation depending on the variable represented by Φ . Convective terms are represented by a third order accurate upwind scheme, and a version of the SIMPLEC (Semi-Implicit Method for Pressure-Linked Equations Consistent) algorithm is used in the solution procedure [17]. Table 2 lists the transport coefficients, Γ^Φ , and the source terms, S^Φ , of the governing equations. For upward non-isothermal flow in a vertical tube, buoyancy forces are included in the simulations, and the gravity vector is in the opposite direction of the flow.

Table 2. Source Term and Transport Coefficients Appearing in Equations (6)-(7)

Φ	Γ^Φ	S^Φ
u	$\mu + \mu_t$	$-\frac{\partial P}{\partial z} + \frac{\partial}{\partial z} \left(\Gamma^u \frac{\partial u}{\partial z} \right) + \frac{\partial}{\partial r} \left(\Gamma^u \frac{\partial v}{\partial z} \right) + \frac{\Gamma^u}{r} \frac{\partial v}{\partial z} + \rho g$
v	$\mu + \mu_t$	$-\frac{\partial P}{\partial r} + \frac{\partial}{\partial z} \left(\Gamma^v \frac{\partial u}{\partial r} \right) + \frac{\partial}{\partial r} \left(\Gamma^v \frac{\partial v}{\partial r} \right) + \frac{\Gamma^v}{r} \frac{\partial v}{\partial r} + 2\Gamma^v \frac{v}{r^2}$
k	$\mu + \frac{\mu_t}{\sigma_k}$	Standard $k-\epsilon$, $G - \rho \epsilon$ Low Re $k-\epsilon$, $C_{\epsilon_1} f_1 \frac{G \epsilon}{k} - C_{\epsilon_2} f_2 \rho \frac{\epsilon^2}{k} + E$
ϵ	$\mu + \frac{\mu_t}{\sigma_\epsilon}$	Standard $k-\epsilon$, $C_1 G \frac{\epsilon}{k} - C_2 \rho \frac{\epsilon^2}{k}$ Low Re $k-\epsilon$, $C_1 G \frac{\epsilon}{k} - C_2 \rho \frac{\epsilon^2}{k}$
h	$\frac{k}{c_p} + \frac{\mu_t}{\sigma_h}$	0
Y_i	$\rho D_i + \frac{\mu_t}{\sigma_{Y_i}}$	$\dot{\omega}_i$

$$G = \mu_t \left[2 \left\{ \left(\frac{\partial u}{\partial z} \right)^2 + \left(\frac{\partial v}{\partial r} \right)^2 + \left(\frac{v}{r} \right)^2 \right\} + \left(\frac{\partial v}{\partial z} + \frac{\partial u}{\partial r} \right)^2 \right]$$

$f_1 = 1.0$, $f_2 = 1 - 0.22 \exp[-(\text{Re}/6)^2]$, $E = -2\nu(\epsilon/y^2) \exp(-0.5 y^+)$, $D = 2\nu k/y^2$, $C_{\epsilon_1} = 1.35$, $C_{\epsilon_2} = 1.8$, $\mu_t = C_\mu \rho k / \epsilon$,

For the development of a thermal oxidative model, it is important to simulate the fluid dynamics and chemistry for different fuels and a range of flow and thermal conditions. Table 3 describes three experiments that measure dissolved O₂ consumption over a range of flow rates (residence times) and are used for comparison with numerical simulations. In research performed elsewhere, Experiment I used isothermal (185 °C) laminar conditions (Reynolds numbers vary from 40 at the inlet to 380 at the tube exit.) within a heated tube (2.16-mm ID x 3.18-mm OD, heated length 0.813 meter) [5, 15, 18]. The interior surface of the tube was either stainless-steel (SS304) or was treated with a passive layer (Silcosteel). Because of its relatively simple flow conditions, Experiment I was also used to “calibrate” the current mechanism. Experiment II from our previous work used a horizontal tube with an imposed wall temperature profile [4]. In Experiment II, the surface contacting the fuel was stainless-steel (SS316), and the horizontal flow transitioned from laminar to turbulent flow (Reynolds numbers vary from 90 at the inlet to 2500 at the tube exit).

Table 3. Experiments used for Simulations

Experiment	Experiment I Isothermal flowing test rig [5, 15, 18]	Experiment II Non isothermal Horizontal flow rig [4]	Experiment III Non isothermal Vertical flow rig (current experiments)
Fuel	Jet A-1 (F2747), Jet A (F3219), Exxsol D110	Jet A-1 (F2747)	Jet A (F3219)
Flow Direction	Horizontal	Horizontal	Vertical upward
Surface	Treated or untreated (SS304)	Untreated (SS316)	Treated or untreated (SS316)
Wall Temperature	185 °C	Varies along tube length	Varies along tube length
Bulk Exit Temperature	185 °C	150 – 300 °C (Varies with wall temperature profile)	150 – 225 °C (Varied with wall temperature profile)
Inlet Flow Rate (ml/min)	1-40	16	20
Pressure (MPa)	2.3	2.48	4.5
Inlet Reynolds No.	20-80	90-150	120-180
Exit Reynolds No.	380-450	1100-2500	1200-2800
Residence Time	0.5 – 3 (min)	7 (sec)	11 (sec)

In the third experiment performed in the present study, the wall temperature profile was imposed on treated (Silcosteel) or untreated (SS316) tubes. The fuel flowed vertically upward and, thus, was assisted by buoyancy forces. As in Experiment II, there was a transition from laminar to turbulent flow (Reynolds number of 120 at the inlet to 2800 at the tube exit). For a numerical simulation to be useful, it is important to show that different fuel samples can be used.

In the current work, the thermal properties (density, viscosity, thermal conductivity, specific heat and enthalpy) of JP-8 and Jet A are assumed to be identical and reasonably represent the properties of Exxsol D110 in the simulations [16]. For the vertically upward flow of Experiment III, when the Reynolds number is greater than 2000, a low Reynolds number $k-\varepsilon$ turbulence model is applied in the computation [19]. The low Reynolds number $k-\varepsilon$ model used in the turbulent simulations allows the integration of the momentum and the $k-\varepsilon$ equation from the tube center to the wall. Moreover, this turbulence model includes the effects of molecular viscosity in the nearsurface regions, which is important for the study of surface reactions at the heated tube wall. For the horizontal flow of Experiment II, the standard $k-\varepsilon$ turbulence model was used when the Reynolds number is greater than 2000. In previous work, use of the standard $k-\varepsilon$ turbulence model resulted in simulations of the fuel temperature and dissolved O₂ consumption that captured the early transition from laminar to turbulent flow and agreed well with measurements [4]. Values of the constants used in the model of turbulent species transport are listed in the nomenclature. Wall temperatures for the non-isothermal conditions were imposed using polynomial fits of the experimental thermocouple measurements. The inlet velocity and temperature profiles were assumed to be uniform for simplicity, and the inlet temperature was taken as 20 °C.

Figure 1 shows the axisymmetric computational grid used in the present work. The grid density used in the simulations was 180 (axial cells) x 15 (radial cells) for the isothermal experiments (Experiment I), 90 (axial cells) x 15 (radial cells) for horizontal flow conditions (Experiment II), and 200 (axial cells) x 15 (radial cells) for vertically upward flow (Experiment III). Further grid refinement resulted in negligible changes in the solutions. The computational grid is clustered near the wall, and the first cell is located at a y^+ distance less than 5. In this work, the deposition process itself is not simulated. Since the surface deposits are thin here, they are assumed to have a negligible influence on heat transfer and flow.

Table 4 shows initial concentrations of species used in the simulations. In Table 4, the small initial concentration of species I used in the present model is 4.0×10^{-8} mol/L as used by Ervin and Zabarnick [4]. An initial dissolved O₂ concentration of 70 ppm ($\sim 1.8 \times 10^{-3}$ mol/L) is assumed for the sample of Exxsol D110, Jet A-1 (F2747), and Jet A (F3219) [4]. Depending on the fuel type, the concentration of antioxidant AH of sample fuels is varied from 0 mol/L to 1.14×10^{-4} mol/L.

Table 4. Initial Concentrations of Species

Species (mol/L)	Initial Concentration
I	4.0×10^{-8}
RH	4.7
O ₂	1.8×10^{-3} (70 ppm)
AH	varied 0 – 1.14×10^{-4} (~ 25 mg/L)
Remaining species are set to 0	

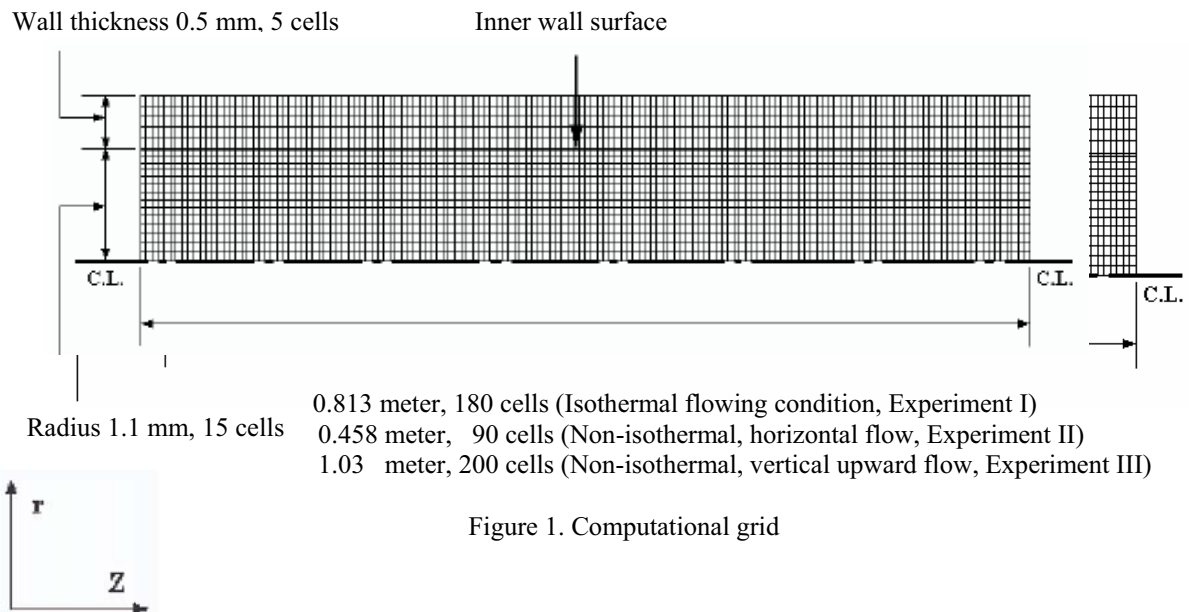


Figure 1. Computational grid

The flow rate was maintained constant at 20 ml/min. Thermocouples welded to the outer surface of the tubing provided wall temperatures along the tube length, and the bulk fuel temperature at the tube outlet was measured (uncertainty of ± 10 °C). The exit bulk temperature of the fuel was varied from 150 °C (maximum wall temperature of 198 °C) to 225 °C (maximum wall temperature of 310 °C) by adjusting the furnace power. Dissolved O₂ levels were measured at the furnace outlet by a modified gas chromatograph. Additional details of the experimental apparatus may be found in the work of Ervin et al. [20].

3. Experimental

To provide further validation of the mechanism used in the present work, experiments (Experiment III, Table 3) were conducted using Jet A fuel (F3219) flowing vertically upward within a tube (2.16-mm ID x 3.18-mm OD) that was heated by a furnace. The surface contacting the fuel was either stainless-steel (SS316, ASTM grade A269/A213, surface roughness 8-15 micro inches) or was stainless-steel treated with a passive layer which involves the chemical vapor deposition of a proprietary silica-based layer (Silcosteel). The silica coating has a nominal thickness of 10,000 angstroms and, thus, does not significantly influence the heat transfer from the wall to the fuel.

4. Results and Discussion For model validation and improved fundamental understanding, it is beneficial to show how computational fluid dynamics combined with the current kinetic mechanism simulates measured dissolved O₂ consumption for different flow conditions, fuels, and surface materials.

4.1 Studies of Exxsol D110 under Isothermal Conditions.

Since Exxsol D110 is a less complex mixture of hydrocarbons than a real jet fuel, the thermal-oxidative behavior of Exxsol D110 is easier to understand than that of a real jet fuel. Exxsol D110 is believed to contain minimal concentrations of antioxidants. In past isothermal flowing experiments, the concentration of BHT was varied to study how the concentration of this antioxidant affects the rate of dissolved O₂ consumption [15]. In numerical simulations, AH can be used to represent BHT. Thus, the measured oxidation rate of Exxsol D110 containing different concentrations of antioxidant, AH, can be used to assess the present simulations (Table 3, Experiment I, variable flow rate). Figure 2 shows measurements and predictions of dissolved O₂ concentration at the heated tube exit for Exxsol D110 containing different concentrations of BHT [15]. All measurements in Figure 2 were performed using a treated tube (wall temperature of 185 °C). Figure 2 shows that the present mechanism which includes a wall reaction reasonably predicts the oxidation rate of Exxsol D110 for concentrations of BHT between 0 mg/L and 25 mg/L. As the concentration of BHT increases, Figure 2 shows that both the measured and simulated oxidation rates of Exxsol D110 decrease. Figure 2 shows that the measured oxidation rates of Exxsol D110 containing 12 mg/L and 25 mg/L of BHT are similar to those of the Jet A-1 (F2747) and Jet A (F3219) fuel samples, respectively [5, 18]. These concentrations of BHT are used to represent the initial concentration of AH for Jet A-1 (F2747, 5.45×10^{-5} mol/L), and Jet A (F3219, 1.14×10^{-4} mol/L) in all simulations of jet fuel which follow. Moreover, since the Jet A-1 sample is hydrotreated, it is reasonable that the simulated value of AH is lower than that of the Jet A fuel.

Fuel F2747 is similar to Exxsol D110 in that the naturally occurring antioxidants have been removed during hydrotreating at the refinery with an antioxidant (or antioxidants) being later added. The addition of a single or small number of synthetic antioxidants would give rise to the observed slow oxidation followed by a rapid increase in oxidation rate once the antioxidant is consumed. Fuels with naturally occurring inhibitors contain a large number of these species which each have somewhat different reactivities. The result is that when the most easily oxidized species is consumed, a second slightly less easily oxidized species is consumed next. This can continue for many species. In addition, several species can be oxidizing, and therefore acting as antioxidants, simultaneously. The result is that the dissolved O₂ consumption curve for fuel F3219 has a more linear shape than the curves for Exxsol D110 and fuel F2747. This more linear O₂ consumption behavior of fuel F3219 could be better duplicated by adjusting AH and SH correctly to fit the O₂ measurements for fuel F3219. However, fitting the complex O₂ consumption behavior of the straight-run fuel F3219 is not a goal of the current work. In addition, fuel sample F2747 (like Exxsol D110) essentially does not contain reactive sulfur species (SH, for example), which is in contrast to fuel F3219. Research is ongoing in developing measurement techniques for different AH and SH species which we desire to add to the current model.

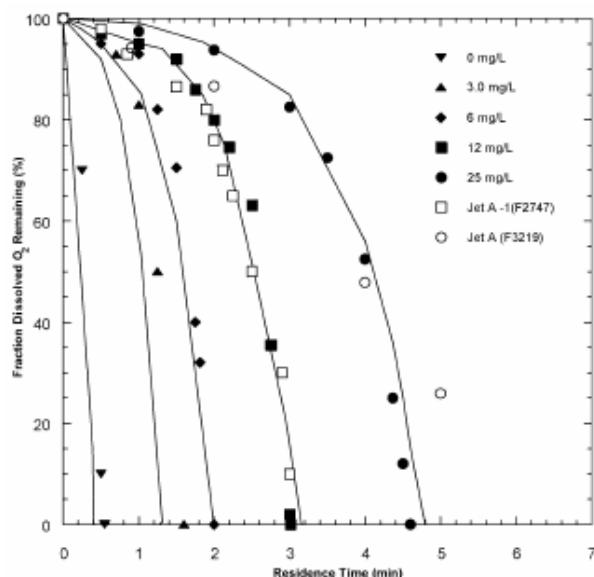


Figure 2. Measured and simulated fraction of dissolved O₂ remaining at the heated tube exit for Exxsol D110 containing different concentrations of BHT [15]. In addition, dissolved O₂ consumption measurements for fuel samples F2747 and F3219 are shown [5, 18]. The flow is isothermal within the treated tube (Experiment I, wall temperature of 185 °C).

4.2 Studies of Jet A-1 (F2747) under Isothermal Conditions. Figure 3 (Experiment I, variable flow rate) compares measured and simulated oxidation of fuel F2747 for stainless-steel and treated tubes for

laminar flow. Figure 3 shows that for the stainless-steel tube the simulated dissolved O₂ concentration is completely consumed after a residence time of 1.8 minutes. For the passivated tube (surface activation energy of 42 kcal/mol), the predicted dissolved O₂ concentration is depleted after an average residence time of 3.25 minutes. Thus, the calculated oxidation rate is reduced for the treated surface. Moreover, Figure 3 shows that the prediction of dissolved O₂ consumption for fuel sample F2747 within isothermal laminar flow conditions agrees reasonably well with the measurements for both passive and active surfaces. The concentration of AH that provides reasonable O₂ consumption rates for fuel F2747 in simulations was established in the Exxsol D110 studies. In addition, the oxidation rate of the Jet A-1 (F2747, hydrotreated) fuel sample was previously measured within either treated (Silcosteel) or untreated tubes (SS304) under isothermal flowing conditions (185 °C) [5]. Thus, the set of measurements for dissolved O₂ consumption for fuel flowing within the untreated tubes can be used to determine the activation energy for the surface reaction occurring on a stain-steel surface. By adjusting the activation energy for reaction 18, it was found that a surface activation energy of 37 kcal/mol provided reasonable agreement between measured and simulated oxidation rates. This value of the surface reaction activation energy is used in all simulations which follow that involve stainless-steel (304 or 316).

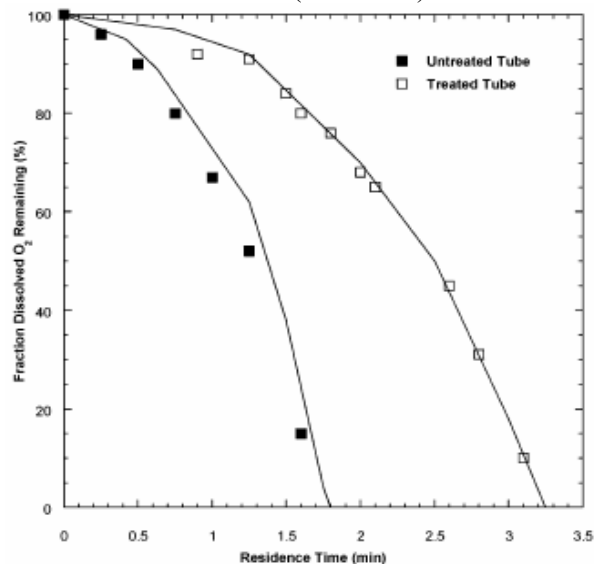


Figure 3. Measured and simulated dissolved O₂ fraction remaining for Jet A-1 fuel (F2747) for isothermal flow (Experiment I, wall temperature of 185 °C) within treated (42 kcal/mol) and untreated tubes (37 kcal/mol) [5].

4.3 Thermal Oxidation of Jet A-1 (F2747) under Non-Isothermal Flowing Conditions. Because fuel oxidation is influenced by the temperature profile within the fuel and the level of turbulence and concomitant mixing, it is important to simulate oxidation within a turbulent flow and under different temperature

conditions. In Table 3, a second set of experimental conditions (Experiment II) which involve the non-isothermal flow of fuel F2747 are shown. In these experiments detailed elsewhere, the tube (SS 316, 0.46 meter long) is horizontal and clamped within a copper block which contains embedded cartridge heaters [4]. Thus, a wall temperature profile is imposed by the heated copper block. For Experiment II, the inlet volumetric flow rate is 16 ml/min. Under these thermal and flow conditions for a horizontal orientation, buoyancy has been shown to produce a premature transition from laminar to turbulent flow [4]. To obtain a range of bulk temperatures at the tube exit, different wall temperature profiles are imposed by adjusting the power input to the heaters. Figure 4 shows measured and simulated fractions of dissolved O₂ remaining at the exit of the tube for F2747 flowing at 16 ml/min for different bulk exit temperatures. Figure 4 shows that the predicted dissolved O₂ begins to be consumed at a bulk exit temperature of 180 °C which is more than 10 °C higher than the temperature corresponding to initial consumption of the measured dissolved O₂. Despite the initial delay associated with the simulated dissolved O₂ consumption, Figure 4 shows that the overall predicted dissolved O₂ behavior agrees reasonably well with the measurements. Moreover, Figure 4 shows that the measured and predicted temperatures associated with O₂ depletion agree well.

4.4 Thermal Oxidation of Jet A Fuel (F3219) under Non-Isothermal Flowing Conditions. Since different fuel samples can have very different thermal-oxidative properties, it is important to perform simulations of different fuel samples flowing over different surface types. Thus for simulations of the third set of experiments (Table 3), a straight-run Jet A fuel (F3219) is selected. This fuel is believed to contain a higher concentration of antioxidants and is a slower oxidizing fuel sample relative to F2747. As described earlier, the wall temperature varies continuously along the tube length for experiments involving fuel F3219. Figure 5 shows measured and predicted dissolved O₂ concentrations for Jet A (F3219) for several outlet bulk temperatures for an entrance flow rate of 20 ml/min. With the more active surface (SS 316), the dissolved O₂ is consumed more rapidly than with the treated tube as observed for Exxsol D110 and fuel F2747. Figure 5 shows that the predicted dissolved O₂ concentration is completely consumed at the tube exit when the bulk temperature there is 216 °C for the untreated tube and 230 °C for the treated tube. Figure 5 shows that simulations of dissolved O₂ consumption for both surface types agree reasonably well with measurements despite the relatively slower consumption predicted at relatively high dissolved O₂ concentrations (80%-100%) for both tube surfaces. Nevertheless, Figure 5 also shows that the trends of the simulated oxidation rates obtained from using the present kinetic mechanism are correct.

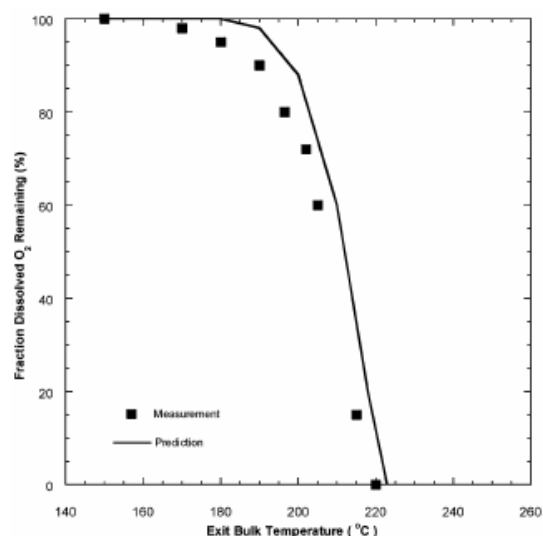


Figure 4. Fraction of O₂ remaining at the exit of the tube (Experiment II, Flow rate 16 ml/min, Fuel Sample F2747).

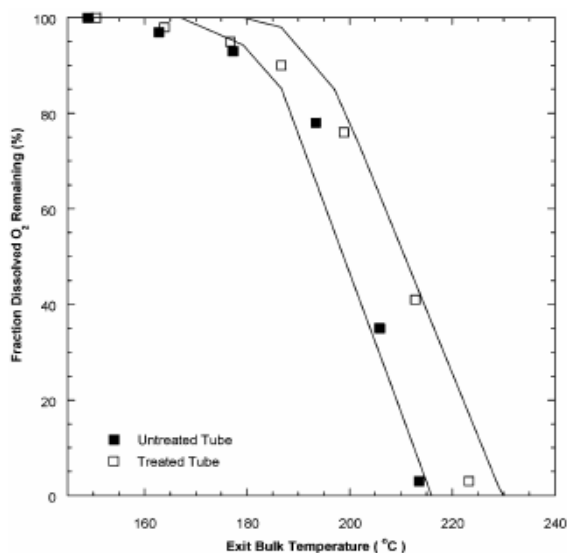


Figure 5. Measurement and simulation of the fraction of dissolved O₂ remaining at the tube exit for Jet-A (F3219) fuel under nonisothermal flowing conditions (Experiment III). Treated (42 kcal/mol) and untreated tubes (37 kcal/mol) tubes with varied exit bulk temperatures for a constant flow rates of 20 ml/min.

5. Conclusions In the present study, the effects of the treated and untreated surfaces on liquid phase thermal-oxidation of different fuel samples were simulated for both isothermal and non-isothermal heated tube experiments using computational fluid dynamics and pseudo-detailed chemical kinetics with a surface reaction. The effects of the surface material on thermal-oxidation were simulated by using different activation energies for the fuel ROOH surface decomposition reaction for different surface materials (42 kcal/mol for treated and 37 kcal/mol for untreated stainless-steel surfaces).

The oxidation measurements and simulations together show that the chemical reactions that occur at the tube surface influence the oxidation rate of jet fuels. Surface passivation has a marked effect in slowing the rate of dissolved O₂ consumption. Comparisons between measurements and simulations of dissolved O₂ consumption on treated and untreated surfaces show that computational fluid dynamics incorporating pseudo-detailed chemical kinetics with the selected wall reaction provides reasonable predictions of dissolved O₂ consumption for jet fuel. Although the chemistry occurring at the heated surface is complex, the influence of the surface material on the thermal oxidation of jet fuel can be reasonably simulated by the inclusion of a surface fuel hydroperoxide decomposition reaction.

Acknowledgments

This work was supported by the U.S. Air Force, Fuels Branch, Propulsion Directorate, Air Force Research Laboratory, Wright-Patterson AFB, OH under contract No. F33615-97-C-2719 and by the Dayton Area Graduate Studies Instituted under grant PR-00-UD-12. The authors would also like to acknowledge Lori M. Balster for measuring dissolved oxygen consumption in an isothermal flow experiment.

References

- [1] Zabarnick, S., 1998. Energy & Fuels, vol. 12, pp. 547-553.
 [2] Ervin, J.S., Zabarnick, S., Williams, T.F., 2000. J. Energy Res. Tech., vol. 122, pp. 229-238.
 [3] Zabarnick, S., 1993. Ind. Eng. Chem. Res., vol. 32, pp. 1012-1017.
 [4] Ervin, J.S., Zabarnick, S., 1998. Energy & Fuels, vol. 12, pp. 344-352.
 [5] Jones, E.G., Balster, L.M., Balster, W., 1996. J. Energy & Fuels, vol. 10, pp. 813-836.
 [6] Silcosteel tubing, Restek Corp., 1998. Bellefonte, P.A., USA.
 [7] Masel, R.I., 1996. Principle of Adsorption and Reaction on Solid Surfaces, Wiley: New York, USA. [8] Anderson, A.W., 1997. Physical Chemistry of Surfaces, Wiley: New York, USA.
 [9] Myers D., 1999. Surfaces Interface and Colloids, Principle and Application, Wiley: New York, USA.
 [10] Coltrin, M.E., Kee, R.J., Rupley, F.M., Meeks, E., 1996. Surface Chemkin-III: A Fortran Package for Analyzing Heterogeneous Chemical Kinetics At a Solid-Surface-Gas-Phase Interface, Sandia National Laboratory, SAND96-8217.
 [11] Stoltze, P., 2000. Progress in Surface Science, vol 65, pp. 65-150.
 [12] Hiatt, R., 1968. J. Org. Chem., vol. 33, pp. 1416-1441.
 [13] Jones, E.G., Balster, W.J., Pickard, J.M., 1996. Trans. ASME J. Eng. Gas Turbines Power, vol. 118, pp. 286-291.

- [14] Jones, E.G., Balster, W.J., Rubey, W.A., 1995. Prep. Am. Chem. Soc., Div. Pet. Chem, vol. 40, pp. 655-659.
 [15] Jones, E.G., Balster, L.M., 2000. Energy & Fuels, vol. 14, pp. 640-645.
 [16] Coordinating Research Council-Handbook of Aviation Fuels Properties, 1983, Atlanta, GA, USA, pp. 22-34.
 [17] CFD Research Corporation, 1998. CFD-ACE Theory Manual Version 5.0, Huntsville, AL., USA.
 [18] Private communication. March 2003. Lori Balster.
 [19] Chien, K.Y., 1982. AIAA Journal, vol. 20, pp. 33-38.
 [20] Ervin, J.S., Ward, T., Williams, T.F., Bento, J., 2003. Energy & Fuels, vol. 17, pp. 577-586.

Nomenclature

C_1	Constant = 1.44
C_2	Constant = 1.92
C_{e_1}	Constant = 1.35
C_{e_2}	Constant = 1.8
C_μ	Constant = 0.09
D_i	Diffusion coefficient of i-th species, m ² /s
f_μ	= $1 - \exp(-0.0115 y^+)$ for Low Reynolds number $k-\varepsilon$, = 1.0 for Standard $k-\varepsilon$
g	Gravitational acceleration, m/s ²
h	Enthalpy, kJ/kg
k	Thermal conductivity, W/m-K; Turbulent kinetic energy, kJ/kg
p	Pressure, MPa
S^Φ	Source term
u	Axial velocity component, m/s
u_τ	Friction velocity, $(\tau_w/\rho)^{1/2}$, m/s
v	Radial velocity component, m/s
$\dot{\omega}_i$	Rate of Production of i-th species, kg/m ³ .s
y	Normal distance from wall, m
y^+	Dimensionless distance from wall, $\rho y u_\tau / \mu$
Y_i	Mass fraction of i-th species
z	Axial coordinate, m
Φ	Assigned variable in equations (1)-(2)
Γ^Φ	Transport coefficient
ε	Dissipation rate, kJ/kg.s
ρ	Density, kg/m ³
σ_k	Constant = 1.0
σ_ε	Constant = 1.3
σ_h	Constant = 1.0
σ_{Y_i}	Constant = 1.0
μ	Absolute viscosity, N.s/m ²
μ_t	Turbulent viscosity, $(C_\mu f_\mu \rho k^2)/\varepsilon$, N.s/m.